HHS Public Access

Author manuscript

J Neurosci Methods. Author manuscript; available in PMC 2016 November 30.

Published in final edited form as:

J Neurosci Methods. 2015 November 30; 255: 122–130. doi:10.1016/j.jneumeth.2015.08.016.

Combining Micro-Computed Tomography with Histology to Analyze Biomedical Implants for Peripheral Nerve Repair

Tracy M. Hopkins[1], **Alexander M. Heilman**[1], **James A. Liggett**[1], **Kathleen LaSance, CNMT, ARRT(N)**[2], **Kevin J. Little, MD**[3], **David B. Hom, MD, FACS**[4], **Danielle M. Minteer, PhD**[5], **Kacey G. Marra, PhD**[6], and **Sarah K. Pixley, PhD**[1,*]

[1]Dept. of Molecular and Cellular Physiology, Univ. of Cincinnati College of Medicine

[2]Director, Vontz Core Imaging Lab (VCIL), University of Cincinnati College of Medicine

[3]Assistant Professor, Division of Pediatric Orthopaedics, Cincinnati Children's Hospital Medical Center

[4]Professor and Director, Division of Facial Plastic & Reconstructive Surgery, Program Director for the Facial Paralysis Clinic, Department of Otolaryngology-Head and Neck Surgery, University of Cincinnati College of Medicine

[5]Dept. of Bioengineering, Univ. of Pittsburgh

[6]Professor, Depts. of Plastic Surgery & Bioengineering, University of Pittsburgh, Director, Plastic Surgery Research Laboratory, Faculty, McGowan Institute for Regenerative Medicine

Abstract

Background—Biomedical implants used in tissue engineering repairs, such as scaffolds to repair peripheral nerves, can be too large to examine completely with histological analyses. Micro-computed tomography (micro-CT) with contrast agents allows ex vivo visualization of entire biomaterial implants and their interactions with tissues, but contrast agents can interfere with histological analyses of the tissues or cause shrinkage or loss of antigenicity.

New Method—Soft tissue, ex vivo micro-CT imaging using Lugol's iodine was compatible with histology after using a rapid (48 h) method of removing iodine.

Results—Adult normal and repaired rat sciatic nerves were infiltrated ex vivo with iodine, imaged with micro-CT and then the iodine was removed by incubating tissues in sodium thiosulfate. Subsequent paraffin sections of normal nerve tissues showed no differences in staining with hematoxylin and eosin or immunostaining with multiple antibodies. Iodine treatment and removal did not alter axonal diameter, nuclear size or relative area covered by immunostained axons ($p>0.05$). Combining imaging modalities allowed comparisons of macroscopic and

[1]Corresponding Author and site of work: Sarah K Pixley, PhD, Associate Professor, Dept. of Molecular and Cellular Physiology, University of Cincinnati Medical Center, Medical Sciences Building (MSB) Rm 4206A, 231 Albert B. Sabin Way, Cincinnati, OH 45267-0576, Tel#: (513) 558-6086, Fax#: (513) 558-5738, Sarah.pixley@uc.edu.

*Portions of this work have appeared previously in abstract and poster format

microscopic features of nerve tissues regenerating through simple nerve conduits or nerve conduits containing a titanium wire for guidance.

Comparison with Existing Methods;—Quantification showed that treatment with iodine and sodium thiosulfate did not result in tissue shrinkage or loss of antigenicity.

Conclusions—Because this combination of treatments is rapid and does not alter tissue morphology, this expands the ex vivo methods available to examine the success of biomaterial implants used for tissue engineering repairs.

Graphical Abstract

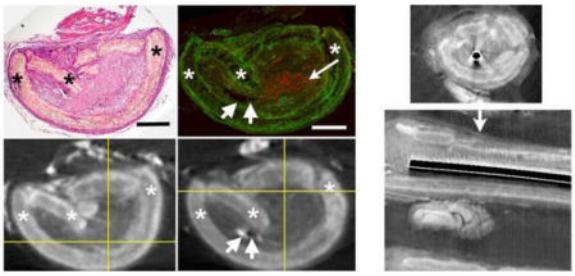

Keywords

Micro-CT; iodine; sodium thiosulfate; Lugol's; immunostaining; tissue engineering; peripheral nerve regeneration; biomedical implants

1 Introduction

Biomedical implants are of significant interest in tissue engineering and medical repairs. The pre-clinical work that is crucial for proceeding to translation involves careful evaluation of the implant, including determining its efficacy in supporting repair, how well the implant integrates into the tissue location and how the tissues respond to the implant. If the implant is biodegradable, then the extent of degradation and tissue reactions to the degradation products must also be evaluated, at both the macroscopic and microscopic levels. Because most surgical implants are relatively large compared to cellular dimensions, then in pre-clinical trials only a small portion of the implant can reasonably be sampled by the normal destructive methods used for histological analyses. Nerve repair is a good example of this because nerves are long, thin, cylindrical structures and repairs can involve nerve gaps of up to several centimeters in length. Histological sectioning, especially in the axial plane, would require significant resources to thoroughly examine the entire implant. Our research focuses on using biomaterial scaffolds to repair injured peripheral nerves, to identify alternatives to autografts, the current gold standard in nerve repair, because autograft use requires additional surgery and nerve loss and current results still do not result in complete restoration of function (Kuffler. 2009; Pfister et al. 2011; Kuffler. 2014). Research has shown that nerve repair is functionally possible using biomaterial nerve conduits (hollow nerve guides) to connect gaps in nerves by placing the cut nerve stumps into the conduits, but only if the nerve gaps are smaller than 2 cm; autografts are still required for longer nerve injury gaps (~2.5 cm or greater) (Pfister et al. 2011; Kuffler. 2014). Thus, research is

ongoing to overcome this clinical limit. Studies in adult rats focus on repairs of the sciatic nerve, which has diameter of around 1–2 mm, and a maximal possible repair length of ~2.8 cm. Random or limited sampling using histological means introduces the potential to miss important features, such as breaks in the conduit, identification of the presence of a continuous strand of regenerating tissues, or identification of the front of incompletely regenerated tissues.

Non-histological imaging techniques are increasingly being used to study nerve regeneration, and some are able to be used in living animals, including magnetic resonance imaging (MRI), diffusion tensor imaging (DTI), ultrasound (US) and positron emission tomography (PET) imaging (Rangavajla et al. 2014; Tseng et al. 2014). Micro-CT imaging has been used far less frequently, because most nerve repair scaffolds and conduits are not dense enough to scatter x-rays. It is possible to use micro-CT on soft tissues (after animal sacrifice) if the tissues are infiltrated with contrast reagents, giving excellent differentiation of different types of soft tissues, as shown in recent studies where multiple reagents were compared (Metscher. 2009a; Metscher. 2009b; Degenhardt et al. 2010). This technique can more readily provide a greater resolution per time of imaging than the other techniques and can be cheaper and easier to access than MRI techniques, which are the ones providing the next best resolution (Rangavajla et al. 2014). We explore here the use of one of these contrast reagents, elemental iodine, for micro-CT imaging of nerves and nerve injury repairs using biomaterial implants.

While useful, the use of contrast reagents for soft tissue micro-CT imaging can add additional challenges. Three relatively well-studied contrast agents are osmium, phosphotungstic acid and elemental iodine. Direct comparisons showed that iodine gave the best rate of tissue infiltration without losing tissue differentiation, it does not require toxic waste disposal and the depth of penetration is greatest, even fully penetrating structures that are10s of mm^3 thick (Metscher. 2009a; Metscher. 2009b; Stephenson et al. 2012; Pauwels et al. 2013; Vickerton et al. 2013). A further advantage of iodine is that, if the penetration is incomplete, the tissues can be repeatedly returned to the iodine solution to allow greater penetration (Jeffery et al. 2011). Osmium infiltration for micro-CT has one of the poorest tissue penetration depths (Metscher. 2009a; Gregg and Butcher. 2012). But an advantage of osmium it has been used to combine micro-CT imaging with post-imaging histology at both the light and electron microscopic levels (Handschuh et al. 2013; Sengle et al. 2013; Scheller et al. 2014). With iodine, post-imaging histological studies have been limited, except for very superficial analyses of tissue structure, because iodine treatment renders soft tissues dense and brittle and imparts a yellow color (Jeffery et al. 2011). One group was able to remove iodine from tissues after micro-CT imaging by extensive soaking and rinsing, but the process took many weeks (Stephenson et al. 2012). Thus, because we sought to combine the advantages of micro-CT using iodine as a contrast reagent with subsequent histology, we sought to identify a more optimal method of removing the iodine after imaging.

A frequently used iodine solution employed for tissue contrast is “Lugol’s solution”, in which molecular iodine (I_2) is combined with potassium iodide (KI) in water resulting in formation of the triiodide ion, I_3^-, with an equilibrium constant of 698 at 25°C (Palmer et al. 1984). The triiodide ion, which gives the solution a characteristic blue-black color and the

tissues a yellow color binds differentially to various tissue types, providing excellent contrast in micro-CT imaging (Jeffery et al. 2011). The terminology surrounding Lugol's solution, first described in the 1800's, can be confusing. As classically defined, "Lugol's solution" refers only to the fact that the solution contains a certain amount (weight) of elemental iodine (I_2) and twice that amount of potassium iodine (KI) in water. Lugol's solution has also been termed potassium iodide or IKI (Metscher. 2009b; Jeffery et al. 2011) or I_2KI (Jeffery et al. 2011; Gignac and Kley. 2014). The term Lugol's does not define the concentration (strength) of the components, although several sources, such as Thermo-Fisher, consider that a "5% solution" is normal or full strength. A 5% solution contains 5 grams of elemental iodine (I_2, 5% iodine) and twice that, 10 grams, of potassium iodide (KI, 10% of the iodide ion) dissolved in 100 mL of water. This "5% solution" can also be correctly described as a 15% solution of total or elemental iodine or a 15% solution of I_2KI. Because there is no technically agreed on regular strength, references to Lugol's should always be carefully defined. Strengths of Lugol's solution that give good tissue definition have varied from 0.1% I_2KI (Metscher. 2009b) to as much as 11–12% I_2KI (Kondo et al. 2001; Gignac and Kley. 2014).

To remove iodine from tissues after microCT imaging, we tested rinsing the tissues with the compound sodium thiosulfate (STS), which reacts with and reduces iodine and other halogen compounds (Zimmermann and Latimer. 1939; Asakai and Hioki. 2011). When STS combines with iodine solutions, the thiosulfate ion reduces iodine and the triiodide ion, producing soluble and colorless iodide ions (iodide ions, I^-), which readily wash out of the tissues (Zimmermann and Latimer. 1939; Kondo et al. 2001). Removal and decolorization of Lugol's and other iodine solutions by STS has been utilized previously in many situations, just not for this particular use, to our knowledge.

Treatment with both Lugol's followed by removal with STS does not appear to harm tissues, as suggested by its use in several histological stains, including the Gram stain for bacteria (Sheehan and Hrapchak. 1980). Both compounds are non-toxic enough that they are safe for human ingestion. In fact, Lugol's solution is used to wash the intestinal lining in patients to detect cancerous lesions, because Lugol's readily stains glycogen-rich normal cells but binds poorly to relatively glycogen-poor cancer cells (McCaul et al. 2013; Coda and Thillainayagam. 2014). STS has been used clinically to remove the iodine after application to the intestines of patients, because the iodine alone can cause some tissue and thus intestinal irritation (Kondo et al. 2001). It is also used to block patient's thyroids for multiple imaging techniques in nuclear medicine studies. Another demonstration that these compounds are not damaging was that if STS was used to remove Lugol's solution after being used to fix plankton and algae samples, then this improved the efficiency of subsequent PCR analyses (Auinger et al. 2008).

However, other reports have reported problems with iodine use, with or without STS. First, tissue shrinkage has been reported with Lugol's as a micro-CT contrast agent (Metscher. 2009a; Degenhardt et al. 2010; Vickerton et al. 2013; Buytaert et al. 2014; Gignac and Kley. 2014). Shrinkage has generally been minimized by keeping the total iodine in the solution below 3.75% total iodine (a 1/25 dilution of a 15% IKI solution, which is a classically defined 5% Lugol's solution), which maintains the osmolality near biological levels

(Degenhardt et al. 2010). However, one group reported shrinkage with a 3% total iodine solution (Buytaert et al. 2014). Second, the use of iodine plus STS has been shown to reduce some types of immunostaining in tissue section applications (Facchetti et al. 2000). However, a subsequent report demonstrated that only six out of 75 antibodies showed reduced or eliminated staining after Lugol's and STS treatment (Wan et al. 2003). Because of these potential concerns, we examined the effects of Lugol's treatment followed by STS treatment on nerve tissues to determine if this caused significant shrinkage or loss of antigenicity. We proposed that these treatments, using a 2% Lugol's solution followed by STS removal of the iodine, would not alter tissue and cellular morphology, thus allowing us to combine microCT analysis with histology to improve the ex vivo study of biomedical implants for tissue engineering repairs of nerve gaps.

2 Methods

2.1 Animals and surgical procedures

For quantitative analysis of the effects of iodine and STS on histology, 3 adult male Lewis rats were used. For demonstrating aspects of how micro-CT imaging can be used in conjunction with histology to study biomedical implants, examples are shown of tissues from a companion study in which sciatic nerve gaps were repaired with poly(caprolactone) (PCL) nerve conduits. From this study, which will be described in greater detail elsewhere (manuscript in preparation), tissues from two adult female Lewis rats are shown. All procedures involving animals were approved by the University of Cincinnati Institutional Animal Care and Use Committee and were in accordance with the NIH Guide for the Care and Use of Laboratory Animals (NIH Publications No. 80–23, revised 1996) and the animal housing was accredited by the Association for Assessment and Accreditation of Laboratory Animal Care International.

For the removal of sciatic nerves for quantitative studies, 3 adult rats were euthanized by approved methods and normal nerve tissues were removed. For nerve repair, a nerve gap was created by removing a section (~1 cm) of the right sciatic nerve in each adult rat and the proximal and distal nerve stumps were sutured into a 1.7 cm long section of hollow PCL conduit (internal diameter 0.7 mm, walls approximately 0.3 – 0.4 mm thick) creating a final gap of 1.5 cm, using the same procedures and type of conduit described in previous nerve repair experiments (Kokai et al. 2009; Kokai et al. 2011). One animal was chosen from the "empty conduit" or control group, where the conduit was filled with saline to displace air. The second animal was from the group of animals in which a titanium (Ti) wire (250 μm diameter and 2 cm length, cleaned in alcohol and sterilized by UV light) was inserted into the tissues of both nerve stumps, covered with the conduit and then the conduit was filled with saline. The animals were sacrificed after 14 weeks using approved euthanasia techniques and the conduits containing regenerated tissues and ~3–5 mm of the attached nerve stumps were removed for analysis. No signs of discomfort were observed and further details of the animal behavior and other results will be described elsewhere.

2.2 Tissue processing, Lugol's iodine staining and STS destaining

Dissected tissues were fixed in 4% paraformaldehyde for 72 hours and rinsed in phosphate-buffered saline (PBS). To prepare tissues for micro-CT imaging, the tissues were incubated in a 2% Lugol's iodine solution (6% total iodine, "diluted Lugol's" from Thermo Fisher Scientific, Waltham, MA) for 48 hours at room temperature and then rinsed with PBS. To remove the iodine, nerves were incubated in a solution of 2.5% STS in PBS (Thermo Fisher Scientific, Florence, KY) for 48 hours, and then rinsed in PBS.

To illustrate the removal of Lugol's by STS, normal nerve tissues were sectioned into pieces and treated with Lugol's and then treated with either STS or PBS. For quantitative studies of the effects of Lugol's plus STS on tissues, a single nerve from each of three animals was sectioned into two pieces that were treated in parallel with Lugol's and STS (treated group) or PBS alone (control group). The two nerve pieces were embedded in one paraffin block such that similar areas of the same nerve were adjacent to each other and they were then sectioned and processed identically, as outlined below.

2.3 Micro-CT imaging

Normal nerves and repaired conduits plus nerve stumps were imaged via micro-CT imaging after Lugol's iodine treatment, using an Inveon Multimodality System (Siemens, Knoxville, TN) in the University of Cincinnati Vontz Imaging Core Facility. The nerves were kept moist in PBS during the approximately one hour scan by placing them in a Styrofoam boat, as shown previously (Vennemeyer et al. 2015). It was possible with this machine and this container to image up to 8 conduits in one scan. Samples were scanned at half-degree increments with 384 steps (step and shoot) for 192 degrees. Images were acquired with high magnification and a pixel matrix binning of 2, resulting in an effective voxel size of 17.27 microns, using 80 kVp voltage and 300 μA current, with a 2100ms exposure time and a 25 ms settle time. The Inveon Research Workplace was used for 2D and 3D analysis, for the creation of 3D volume rendered videos, to crop the images of each conduit into separate files and then to export as DICOM files (Digital Imaging and Communications in Medicine, the universal digital format agreed upon for use by all human medical imaging manufacturers). This resulted in axial stacks of up to or over 1,000 images (1 pixel per image, 56.6 pixels per mm) per tissue. DICOM image data was imported into NIH ImageJ as a data sequence and then viewed in 3D using the orthogonal viewing function (Image → stack → orthogonal views). Exporting as DICOM images and using ImageJ for further extensive analysis was advantageous because analysis time using the Inveon software, a proprietary package, was limited in our multi-user center. ImageJ was also used to export images of single axial sections.

2.4 Post-imaging tissue processing and staining

After removal of iodine from tissues using STS, tissues were paraffin embedded, sectioned (7–10 μm thick) and slides with sections were either stained with antibodies or with hematoxylin and eosin (H&E). H&E slides were dehydrated and coverslipped with Permount (Fisher). The immunostaining procedures were as described previously (Vennemeyer et al. 2015), staining for axons (rabbit antibody to the 200 MW neurofilament protein (anti-NF, 1:500 dilution, Sigma, St. Louis, MO), Schwann cells (antibody to the

S100 protein, 1:500, DAKO, Carpenterio, CA), and blood vessel endothelial cells, using TRITC labeled *Bandeiraea simplicifolia* lectin (1:1,000, Sigma L-5264) (Mattsson et al. 2002). Perineurial fibroblasts and endothelial cells within nerves, both of which maintain an intact nerve-blood barrier and transport glucose trans-cellularly, were stained by a mouse monoclonal to the glucose transporter-1 protein (anti-GLUT-1, 1:250 dilution, Thermo, Fremont, CA) (Stark et al. 2000). Cell nuclei were stained with 4′,6-diamidino-2-phenylindole (DAPI, 1:1000 dilution, Sigma, St. Louis, MO). Secondary antibodies were anti-mouse Alexa 488 and anti-rabbit Alexa 594 (1:1000 dilution, Invitrogen, Grand Island, NY), and sections were coverslipped with Fluoromount (Fisher).

2.5 Photography and image analysis of stained tissues

Color pictures of H&E stained sections were photographed on an upright Zeiss Axioplan Imaging 2e fluorescence microscope with a Zeiss Axiocam digital camera. For immunostained sections, grayscale images were taken on the same Zeiss microscope with a QICam cooled CCS camera (Q Imaging, Canada) and pseudo-colored in Photoshop. Quantitative analyses were done using NIH ImageJ or Photoshop. For fluorescence photography, exposure times were set at the same value for similarly stained tissues and any changes in contrast or brightness that were made in Photoshop to make the image more visible for the figure were completely duplicated in the matching photo.

Axon diameters were measured in photomicrographs of H&E stained sections taken with a 100x oil objective (30+ axons per three sections per three rats, paired sections, n=9 pairs). For nuclear area, the area per DAPI stained nucleus was measured in photomicrographs taken with a 40X oil objective of regions only within nerve tissue (6+ nuclei per section, 3 sections per three rats, paired sections, n=9 pairs). With anti-NF axon staining, the area covered by immunostaining per four regions of interest (ROIs = 25 μm^2), in two sections per nerve per three rats, paired sections (n=6 pairs).

2.6 Statistics

Statistical analyses comparing paired nerves from a single animal treated with either Lugol's/STS or PBS treated nerves were done with Sigma Plot 13, using a repeated measures ANOVA, with a *p*-value of <0.05 considered a significant difference.

3 Results

3.1 Imaging Normal Nerves with Iodine and micro-CT

Figure 1 illustrates micro-CT images of normal adult rat sciatic nerves after incubation in Lugol's iodine. The images in Figure 1 were generated using the Inveon Research Workplace software, which provides 2D coronal (XZ), axial (XY) and sagittal (ZY) image slice data. Excellent differentiation was seen between nerve bundles (arrows) and the surrounding tissues, which consisted of primarily skeletal muscle.

3.2 Removal of Iodine

To remove iodine, sections of the normal nerves were placed in either PBS or a solution of sodium thiosulfate (STS). As shown in Figure 2, incubation in STS resulted in a loss of the

iodine coloration that was almost complete by 24 hours (top panels). Soaking in PBS for the same time did not result in any change in tissue coloration (bottom panels). Treatment for further tissue work was set at 48 hours to ensure adequate removal and no traces of iodine were observed in subsequent tissue processing. However, it is possible that longer incubations may be required with a larger structure.

3.3 Analysis of histological and immunohistological staining after Lugol's treatment

To determine the effects of Lugol's iodine and STS treatments on staining, normal sciatic nerves were cut into two pieces and treated in parallel with Lugol's and STS or just PBS rinses. Both sections of nerve were embedded together in paraffin so that the midpoints of both nerves were adjacent to each other on the same slide and thus subjected to the same staining conditions. In Figure 3, tissues in the left column (A, C, E, G, I) were treated with PBS alone and show no significant differences from tissues treated with Lugol's and STS, in the right column (B, D, F, H, J).

Cellular features that could be compared between the images included axons, after staining with H&E, (Fig. 3A and 3B, between the sets of arrows). The axons showed the characteristic eosinophilic dot in the center of clear cellular material that is the myelin sheath (between arrows). With anti-NF staining (red (colors refer to online version, all are white and black in the print version) in 3C and 3D), regularly spaced axonal cross sections and some longitudinal lengths of axons can be seen. With the antibody to S100 protein, Schwann cell staining appears to give circular patterns because staining is primarily in the cytoplasm surrounding the myelinated axon (red/white in 3E and 3F). The fluorescently tagged lectin labels endothelial cells), so multiple small vessels are stained, appearing as either hollows or sections of parallel lines, (red/white in 3G and 3H, arrow), while nuclei are small and ellipsoid and stained blue (fainter white, DAPI staining) in this merged image. In I and J, an antibody to GLUT-1 (green/white) labels the perineurium, which appears here as a line of staining inner to the unstained epineurium (left arrows in I and J) and the endothelial cells of a blood vessel (right arrows in I and J). In this merged view, nuclei are blue (DAPI staining) and red blood cells are red due to enhancing the background staining that appeared in the red channel.

3.4 Quantification of the effects of iodine treatment on tissue morphology

Using the paired treated and untreated nerve sections, cellular measures were quantified to determine if the Lugol's/STS treatment caused shrinkage or swelling compared to PBS treatment. Axonal diameter was quantified in H&E stained sections, nuclear size was analyzed as the area of DAPI staining per region of interest within nerve bundles and axonal "load" within nerve bundles was analyzed as the amount of NF staining area (as a percent of the total image area). The Lugol's/STS treatment did not significantly alter any of these measures ($p>0.05$) and the graphed results are shown in Figure 4. Thus, treating tissues with Lugol's and STS does not appear to result in any significant tissue swelling or shrinkage that is different from PBS treated tissues.

3.5 Use of micro-CT to evaluate bioimplant success and integrity

As part of ongoing research on biomaterial solutions for improving peripheral nerve repair, gaps in the sciatic nerves of adult rats were repaired by reconnecting the separated nerve stumps with PCL nerve conduits. Examples shown here demonstrate some ways in which microCT imaging can be combined with histology to examine both the conduit and the internal regenerating tissues. In Figure 5, images are shown from an animal that received a conduit filled with saline and in Figure 6, images are from an animal that had received a saline-filled conduit placed over a titanium (Ti) wire that contacted both nerve stumps. Tissues had regenerated across the gaps in both conduits after 14 weeks.

In Figure 5, A and B, two micro-CT views are shown of longitudinal reconstructions of one conduit containing regenerating nerve tissues, after Lugol's iodine incubation. These were created in ImageJ from a stack of axial micro-CT images. The conduit (asterisks) can be clearly differentiated from the proximal (left) and distal (right) nerve stumps and the internal regenerating nerve tissues connecting the stumps. The arrow in 5B points to the internal regenerating tissues as they pass through a region where there is a distinct crack in the conduit. Analysis of all images confirmed that the tissues were continuous through the conduit.

After removal of the Lugol's iodine with STS, this same conduit with tissue was paraffin embedded and sectioned in the axial plane, with retention of sections at every 500 μm throughout the entire conduit. Some sections were stained with H&E, as shown in Fig. 5C, while other sections were immunostained for axons (anti-NF (red), Figure 5D, arrow points to a cluster of the axonal cross-sections). The micro-CT images were matched to their respective stained sections. The H&E stained section (Figure 5D) was determined to be closest to axial image 1084, shown in Figure 5E (out of 1427 axial images, numbering starting at the proximal end). The position of this axial slice is marked by the vertical crossbar in the longitudinal image in Figure 5A. The anti-NF stained section in Figure 5D was matched to axial image 1164, which is shown in Figure 5F and marked by the vertical crossbar in Fig. 5B. In the anti-NF stained figure (5D), the contrast in the green channel, which has no specific immunostaining, was adjusted in Photoshop to allow visualization of the unstained tissues surrounding the red-stained axons. Slight differences in the shape of the tissue are seen between the micro-CT and stained images, which suggest that some distortion (i.e. compression) occurred during the tissue processing after micro-CT imaging (which included paraffin embedding, sectioning and staining of tissues). Locating the position of the anti-NF image confirmed that axonal regrowth occurred significantly distal to at least one significant break in the conduit (Fig. 5B, arrow) and that even though there was lower density in the regenerating tissue strand distal relative to proximal in the micro-CT image, there were still nerve fascicles present. The significance of this is that regenerating axons were able to transverse through the entire conduit, despite what appear to be relatively major conduit disruptions. This is just one example of how a more complete analysis is possible by combining these techniques.

To give a measure of the resolution possible in the micro-CT image, two tissue structures are indicated by sets of two short arrows in both Fig. 5D and the corresponding micro-CT image in Fig. 5F. The short arrows on the left in each image point to a small pocket of fat,

which looks blank and unstained in Fig. 5D and bright white in the micro-CT image (Fig. 5F). The short arrows on the right point to a relatively large blood vessel that is faintly stained in D and is a black spot in F. The fat pocket is~386 microns along its longest axis and ~100 microns wide, perpendicular to that axis. The blood vessel internal diameter is ~140 wide by ~52 microns high. The resolution was not, however, sufficient to detect nerve fascicles within the regenerating tissue, even though the histological views showed that nerve fascicles were more densely packed (had less extracellular material) than the surrounding connective tissues inside the conduit.

3.6 Imaging of both dense and soft tissues

In one set of the test animals, a titanium (Ti) wire was placed between the nerve stumps, to determine if it would provide guidance for regenerating nerve tissues, similar to our previous study where a magnesium wire was placed in a conduit (Vennemeyer et al. 2015). With a Ti wire, which cannot be cut with a standard microtome blade, histology is not readily available to examine the tissues inside the conduit, adjacent to the metal. Because the nerves are so small and thin, it also was not possible to remove the metal and have sufficient intact tissue left to analyze, which is how tissues around larger metal implants are analyzed. Using iodine infiltration, it was possible to image the soft tissues around the Ti wire with micro-CT imaging (Figure 6). There were some minimal artifacts in the microCT, due to difference in densities between Ti wire and the soft tissue. These included that the Ti wire appeared as a black object due to over-saturation, there was a shadowing effect that resulted in loss of soft tissue imaging next to the wire on one side and there were scatter artifacts (white lines) in the adjacent soft tissue. However, it was still possible to make out important details like the cracks in the conduit and the fact that there were areas of regenerating tissues detectable running through the entire length of the conduit. This supports the idea that the tissue was able to regenerate through the conduit in the presence of the Ti wire. Thus, with the soft tissue contrast reagent, iodine, we could gather information about the integrity of the conduit and the regenerating tissues around the metal, which would not have been available otherwise.

4 Discussion

4.1 Overview

We have described a relatively rapid method of removing iodine from tissues that makes it possible to combine the imaging of soft tissues by micro-CT with subsequent histological techniques that allow studies of the cellular relationships in the same tissues. We demonstrated that the combination of iodine treatment and its removal did not significantly disrupt tissue morphology or reduce staining capacity for any antibody tested to date. We demonstrate some aspects of how this combination of imaging modalities can be used to study nerve regeneration through biomaterial nerve conduits.

4.2 In vivo imaging techniques

Other methods of imaging other than microscopy or microCT are also being used to study nerve regeneration, either with or without nerve conduits. Of exciting interest are techniques that allow imaging in the living animal. These include magnetic resonance imaging (MRI),

with or without diffusion tensor imaging (DTI), ultrasound (US) and positron emission tomography (PET). US is the least expensive of the techniques, and unlike some MRI techniques, it can allow visualization along the entire length of a regenerating nerve. However, this visualization can be limited by the anatomy of the animal, the nerve cannot be visualized if there are insufficient nearby anatomical landmarks and the resolution is inferior to either MRI or microCT (Tseng et al. 2014; Rangavajla et al. 2014). PET techniques with specific contrast reagents that target injured nerves are showing promise, but are still in their infancy (Rangavajla et al. 2014). Currently, MRI techniques, alone or with DTI, are proving highly valuable for studying peripheral nerve regeneration, as outlined in recent reviews (Tseng et al. 2014; Rangavajla et al. 2014). In particular, MRI has been used to successfully study regenerating sciatic nerves, repaired with or without biomaterial conduits, in living mice (Lehmann et al. 2010), rats (Bendszus et al. 2004; Li et al. 2014; Tremp et al. 2015) and rabbits (Hsu et al. 2011; Yamasaki et al. 2015). Imaging parameters or modalities that are most helpful include T2 weighting, use of various contrast reagents, certain parameters of DTI imaging and, in the case of implantation of cells to aid regeneration, loading the cells with contrast agents (Rangavajla et al. 2014; Tseng et al. 2014; Tremp et al. 2015). These imaging techniques are especially valuable for following nerve repair because they can help locate the regenerating nerve front in live animals. They can also be used to obtain quantitative measures of both the length of the regenerating nerve and the thickness of the conduit in living animals (Hsu et al. 2011).

4.2 Ex vivo imaging techniques

The microCT imaging of soft tissues with iodine that we are describing here is not possible to apply to live animals, so it cannot be used to follow the course of nerve regeneration in a single animal, as is possible with the above techniques. However, we propose that microCT can be a valuable addition to post-sacrifice, ex vivo, analysis. First, the resolution is increased compared to other MRI techniques. For example, the theoretical voxel size of our micro-CT imaging was 17.27 microns, while DTI resolution is around 1.6 mm/voxel (Rangavajla et al. 2014). As shown, we were able to visualize objects as small as <60 micron. This allows a very thorough analysis of the entire structure after dissection, and is definitely sufficient to determine if the tissue is complete throughout a conduit and to find the front of regeneration if it is not complete. The resolution is sufficient to observe some larger histological structures, as shown in Figure 5, although it was not sufficient to differentiate the nerve fascicles, which are slightly denser than the surrounding connective tissues. In the future, it might be possible to add this capacity by using immunostaining techniques that deposit heavy metals on the antigenic structures of interest (Metscher and Müller. 2011).

In terms of ex vivo application of these techniques, micro-CT is generally less expensive than MRI and, while both require trained personnel to assist with imaging and analysis, MRI imaging and processing can require a greater participation by highly skilled personnel.

4.3 Combining techniques

The advantage of adding micro-CT imaging to histology is that histology would take significant time and resources to obtain a completely reconstructed 3D view of an entire

implant. Random sampling in the axial plane could miss breaks in the conduit or other anomalies and could also miss the front of regeneration if there is partial growth into the conduit. Sectioning in the longitudinal plane would allow identification of the nerve front, but this type of sectioning can be challenging because of the often non-linear nature of nerves. With micro-CT imaging, a stack of multiple images is generated that can be studied in 3 planes throughout its length, despite variations in the orientation. Adding micro-CT was especially beneficial when a very dense material, a metal wire, was being studied as a nerve support. There were few other methods of examining the soft tissues adjacent to the wire and inside the conduit.

Another advantage of adding microCT imaging to standard histological studies is that the information from the micro-CT can be used to guide the histological studies. The actual microCT imaging takes approximately an hour and this is done within the first week after sacrifice of the animals. Analysis of the images can be done rapidly thereafter, while the tissues are being paraffin embedded. Thus, information such as the existence of breaks or position of the regeneration front could be used to determine where and how much of the conduit is to be sectioned. This could shorten the time and resources needed for sectioning. The cost of the microCT, which is usually more than US but less than MRI imaging, can be minimized by imaging multiple conduits together, and then these costs might be recovered by the possible reduction in costs of the histological analyses. Further conservation is due to the fact that only one set of animals is needed to do both types of analysis. So using microCT can significantly add to the nature of the analysis and reduce the total animal count and costs of the experiment.

4.4 Conclusions

We propose that applications that could benefit from the combined use of micro-CT and histology include not only nerve repair, but studies of other biomaterial implants. The implants can be denser than tissues, the same as tissues, or they could be mixed material implants containing multiple density materials. Because of the size and complex placement of implants, micro-CT imaging can provide valuable information on the integrity of the entire implant, how it has been impacted by implantation and its relationship with neighboring tissues. Specifically, we show here how micro-CT imaging of a regenerating nerve in a biomaterial conduit identified both axial breakage points along the conduit, as well as breakage of the intact circle of the conduit (Fig. 5), which suggests multiple pressures were exerted on this conduit, perhaps combined with the initiation of degradation. Some of the breakage points might have been missed using just axial histological analyses, because that would have required retaining all, or almost all, serial sections, and then reconstructing the information from those sections, which is not a trivial task. Instead, using standard image analysis software packages, numerous aspects of the conduits can be examined and quantified. This can occur rapidly enough that it can guide subsequent histological analysis. Finally, coupling a macro-level analysis by micro-CT with the power of obtaining microscopic data on the same tissues in the same animals, reduces the number of animals required for any one study. Thus, overall, this combination can substantially expand the study of the success and effectiveness of biomaterial biomedical implants.

Acknowledgments

This research was supported by grants from the NSF ERC for Revolutionizing Metallic Biomaterials (EEC-0812348 and NCAT 260116C supplement) (SP), the American Academy of Otolaryngology, the American Association of Hand Surgeons (AAHS) Annual Research Grant (KL, SP), funding from the University of Cincinnati Department of Otolaryngology-Head and Neck Surgery (MG, DH) and a Just-In-Time grant from an Institutional Clinical and Translational Science Award, NIH/NCATS Grant Number 8UL1TR000077-04, for some of the imaging work, which was done in the UC Vontz Imaging Core Facility. Any opinions, findings, and conclusions or recommendations expressed in this material are those of the authors and do not necessarily reflect the views of any of the funding agencies.

Abbreviations

DAPI	4′,6-diamidino-2-phenylindole
anti-NF	antibody to neurofilament protein 200
DICOM file format	Digital Imaging and Communications in Medicine file format
DTI	diffusion tensor imaging
GLUT-1	the glucose transporter-1 protein
H&E	hematoxylin and eosin
I^-	iodide ions
IKI or I_2KI	iodine potassium iodide
LM	light microscopy
micro-CT	micro-computed tomography
I_2	molecular iodine
MRI	molecular resonance imaging
PBS	phosphate buffered saline
PET	positron emission tomography
PCL	poly(caprolactone)
PCR	polymerase chain reaction
KI	potassium iodide
STS	sodium thiosulfate
TRITC	tetramethylrhodamine isothiocyanate
Ti	titanium
I_3^-	triiodide ion
US	ultrasound

References

Asakai T, Hioki A. Investigation of iodine liberation process in redox titration of potassium iodate with sodium thiosulfate. Anal Chim Acta. 2011; 689:34–38. [PubMed: 21338753]

Auinger BM, Pfandl K, Boenigk J. Improved methodology for identification of protists and microalgae from plankton samples preserved in Lugol's iodine solution: Combining microscopic analysis with single-cell PCR. Appl Environ Microbiol. 2008; 74:2505–2510. [PubMed: 18296536]

Bendszus M, Wessig C, Solymosi L, Reiners K, Koltzenburg M. MRI of peripheral nerve degeneration and regeneration: correlation with electrophysiology and histology. Exp Neurol. 2004; 188:171–177. [PubMed: 15191813]

Buytaert J, Goyens J, De Greef D, Aerts P, Dirckx J. Volume shrinkage of bone, brain and muscle tissue in sample preparation for micro-CT and light sheet fluorescence microscopy (LSFM). Microsc Microanal. 2014; 20:1208–1217. [PubMed: 24963987]

Coda S, Thillainayagam AV. State of the art in advanced endoscopic imaging for the detection and evaluation of dysplasia and early cancer of the gastrointestinal tract. Clin Exp Gastroenterol. 2014; 7:133–150. [PubMed: 24868168]

Degenhardt K, Wright AC, Horng D, Padmanabhan A, Epstein JA. Rapid 3D phenotyping of cardiovascular development in mouse embryos by micro-CT with iodine staining. Circ Cardiovasc Imaging. 2010; 3:314–322. [PubMed: 20190279]

Facchetti F, Alebardi O, Vermi W. Omit iodine and CD30 will shine: A simple technical procedure to demonstrate the CD30 antigen on B5-fixed material [10]. Am J Surg Pathol. 2000; 24:320–322. [PubMed: 10680909]

Gignac PM, Kley NJ. Iodine-enhanced micro-CT imaging: Methodological refinements for the study of the soft-tissue anatomy of post-embryonic vertebrates. J Exp Zool Part B Mol Dev Evol. 2014; 322:166–176.

Gregg CL, Butcher JT. Quantitative in vivo imaging of embryonic development: Opportunities and challenges. Differentiation. 2012; 84:149–162. [PubMed: 22695188]

Handschuh S, Baeumler N, Schwaha T, Ruthensteiner B. A correlative approach for combining microCT, light and transmission electron microscopy in a single 3D scenario. Front Zool. 2013:10. [PubMed: 23496925]

Hsu S, Chan S, Chiang C, Chi-Chang Chen C, Jiang C. Peripheral nerve regeneration using a microporous polylactic acid asymmetric conduit in a rabbit long-gap sciatic nerve transection model. Biomaterials. 2011; 32:3764–3775. [PubMed: 21396706]

Jeffery NS, Stephenson RS, Gallagher JA, Jarvis JC, Cox PG. Micro-computed tomography with iodine staining resolves the arrangement of muscle fibres. J Biomech. 2011; 44:189–192. [PubMed: 20846653]

Kokai LE, Bourbeau D, Weber D, McAtee J, Marra KG. Sustained growth factor delivery promotes axonal regeneration in long gap peripheral nerve repair. Tissue Eng Part A. 2011; 17:1263–1275. [PubMed: 21189072]

Kokai LE, Lin Y, Oyster NM, Marra KG. Diffusion of soluble factors through degradable polymer nerve guides: Controlling manufacturing parameters. Acta Biomaterialia. 2009; 5:2540–2550. [PubMed: 19369123]

Kondo H, Fukuda H, Ono H, Gotoda T, Saito D, Takahiro K, Shirao K, Yamaguchi H, Yoshida S. Sodium thiosulfate solution spray for relief of irritation caused by Lugol's stain in chromoendoscopy. Gastrointest Endosc. 2001; 53:199–202. [PubMed: 11174292]

Kuffler DP. An assessment of current techniques for inducing axon regeneration and neurological recovery following peripheral nerve trauma. Prog Neurobiol. 2014; 116:1–12. [PubMed: 24380784]

Kuffler, DP. Chapter 18 Enhancement of Nerve Regeneration and Recovery by Immunosuppressive Agents. In: Geuna, Stefano; Tos, Pierluigi; Battiston, Bruno, editors. International Review of Neurobiology. Academic Press; 2009. p. 347-362.

Lehmann HC, Zhang J, Mori S, Sheikh KA. Diffusion tensor imaging to assess axonal regeneration in peripheral nerves. Exp Neurol. 2010; 223:238–244. [PubMed: 19879260]

Li R, Hettinger PC, Liu X, Machol J, Yan J, Matloub HS, Hyde JS. Early evaluation of nerve regeneration after nerve injury and repair using functional connectivity MRI. Neurorehabil Neural Repair. 2014; 28:707–715. [PubMed: 24515926]

Mattsson G, Carlsson P, Olausson K, Jansson L. Histological markers for endothelial cells in endogenous and transplanted rodent pancreatic islets. Pancreatology. 2002; 2:155–162. [PubMed: 12123096]

McCaul JA, Cymerman JA, Hislop S, McConkey C, McMahon J, Mehanna H, Shaw R, Sutton DN, Dunn J. LIHNCS - Lugol's iodine in head and neck cancer surgery: A multicentre, randomised controlled trial assessing the effectiveness of Lugol's iodine to assist excision of moderate dysplasia, severe dysplasia and carcinoma in situ at mucosal resection margins of oral and oropharyngeal squamous cell carcinoma: Study protocol for a randomised controlled trial. Trials. 2013:14. [PubMed: 23305191]

Metscher BD. Micro CT for comparative morphology: Simple staining methods allow high-contrast 3D imaging of diverse non-mineralized animal tissues. BMC Physiol. 2009a:9. [PubMed: 19383148]

Metscher BD. MicroCT for developmental biology: A versatile tool for high-contrast 3D imaging at histological resolutions. Dev Dyn. 2009b; 238:632–640. [PubMed: 19235724]

Metscher BD, Müller GB. MicroCT for molecular imaging: Quantitative visualization of complete three-dimensional distributions of gene products in embryonic limbs. Dev Dyn. 2011; 240:2301–2308. [PubMed: 21901786]

Palmer DA, Ramette RW, Mesmer RE. Triiodide ion formation equilibrium and activity coefficients in aqueous solution. J Solution Chem. 1984; 13:673–683.

Pauwels E, Van Loo D, Cornillie P, Brabant L, Van Hoorebeke L. An exploratory study of contrast agents for soft tissue visualization by means of high resolution X-ray computed tomography imaging. J Microsc. 2013; 250:21–31. [PubMed: 23432572]

Pfister BJ, Gordon T, Loverde JR, Kochar AS, Mackinnon SE, Kacy Cullen D. Biomedical engineering strategies for peripheral nerve repair: Surgical applications, state of the art, and future challenges. Crit Rev Biomed Eng. 2011; 39:81–124. [PubMed: 21488817]

Rangavajla G, Mokarram N, Masoodzadehgan N, Pai SB, Bellamkonda RV. Noninvasive imaging of peripheral nerves. Cells Tissues Organs. 2014; 200:69–77. [PubMed: 25766202]

Scheller EL, Troiano N, Vanhoutan JN, Bouxsein MA, Fretz JA, Xi Y, Nelson T, Katz G, Berry R, Church CD, Doucette CR, Rodeheffer MS, MacDougald OA, Rosen CJ, Horowitz MC. Use of osmium tetroxide staining with microcomputerized tomography to visualize and quantify bone marrow adipose tissue in vivo. Methods Enzymol. 2014; 537:123–139. [PubMed: 24480344]

Sengle G, Tufa SF, Sakai LY, Zulliger MA, Keene DR. A correlative method for imaging identical regions of samples by micro-CT, light microscopy, and electron microscopy: Imaging adipose tissue in a model system. J Histochem Cytochem. 2013; 61:263–271. [PubMed: 23264636]

Sheehan, DC.; Hrapchak, BB. Theory and Practice of Histotechnology. St. Louis: The C.V. Mosby Company; 1980.

Stark B, Carlstedt T, Cullheim S, Risling M. Developmental and lesion-induced changes in the distribution of the glucose transporter Glut-1 in the central and peripheral nervous system. Exp Brain Res. 2000; 131:74–84. [PubMed: 10759173]

Stephenson RS, Boyett MR, Hart G, Nikolaidou T, Cai X, Corno AF, Alphonso N, Jeffery N, Jarvis JC. Contrast enhanced micro-computed tomography resolves the 3-dimensional morphology of the cardiac conduction system in mammalian hearts. PLoS ONE. 2012:7.

Tremp M, Zu Schwabedissen MM, Kappos EA, Engels PE, Fischmann A, Scherberich A, Schaefer DJ, Kalbermatten DF. The regeneration potential after human and autologous stem cell transplantation in a rat sciatic nerve injury model can be monitored by MRI. Cell Transplant. 2015; 24:203–211. [PubMed: 24380629]

Tseng T, Yen C, Hsu S. Visualization of peripheral nerve regeneration. Neural Regen Res. 2014; 9:997–999. [PubMed: 25206750]

Vennemeyer JJ, Hopkins T, Hershcovitch M, Little KD, Hagen MC, Minteer D, Hom DB, Marra K, Pixley SK. Initial observations on using magnesium metal in peripheral nerve repair. J Biomater Appl. 2015; 29:1145–1154. [PubMed: 25281648]

Vickerton P, Jarvis J, Jeffery N. Concentration-dependent specimen shrinkage in iodine-enhanced microCT. J Anat. 2013; 223:185–193. [PubMed: 23721431]

Wan X, Cochran G, Greiner TC. Removal of mercuric chloride deposits from B5-fixed tissue will affect the performance of immunoperoxidase staining of selected antibodies. Appl Immunohistochem Mol Morphol. 2003; 11:92–95. [PubMed: 12610363]

Yamasaki T, Fujiwara H, Oda R, Mikami Y, Ikeda T, Nagae M, Shirai T, Morisaki S, Ikoma K, Masugi-Tokita M, Yamada K, Kawata M, Kubo T. In vivo evaluation of rabbit sciatic nerve regeneration with diffusion tensor imaging (DTI): Correlations with histology and behavior. Magn Reson Imaging. 2015; 33:95–101. [PubMed: 25271136]

Zimmermann HW, Latimer WM. The heat of the reaction of thiosulfate with triiodide. J Am Chem Soc. 1939; 61:1554–1555.

Highlights

- Imaged ex vivo iodinated normal and repaired nerves with micro-CT.
- Removed iodine with sodium thiosulfate, allowing subsequent histology.
- Removal of iodine did not alter immunostaining or cellular morphology.
- Matching CT to staining improved studies of nerve regeneration through conduits.
- Micro-CT with iodine allowed imaging of soft tissues adjacent to metal implants

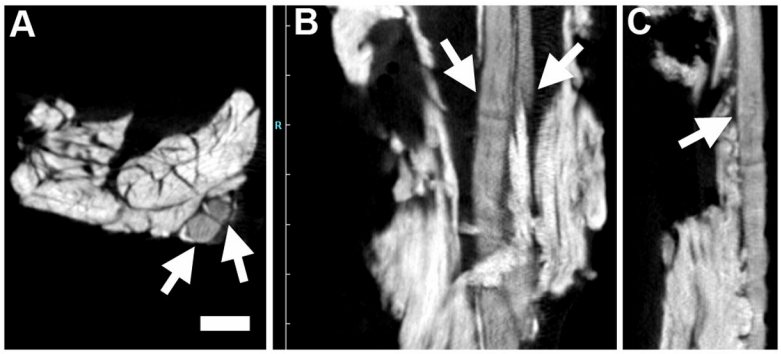

Figure 1.

Normal sciatic nerve infiltrated with iodine and imaged via micro-CT. The micro-CT images of one nerve were serially reconstructed and viewed in A) the axial (cross-sectional) plane (bottom of the scanner bed is at the bottom of the image) and two longitudinal views: B) the sagittal plane and C) the coronal plane (the bottom of the scanner bed is to the left). Arrows point to nerve tissue. Bar = 1 mm and applies to all three panels.

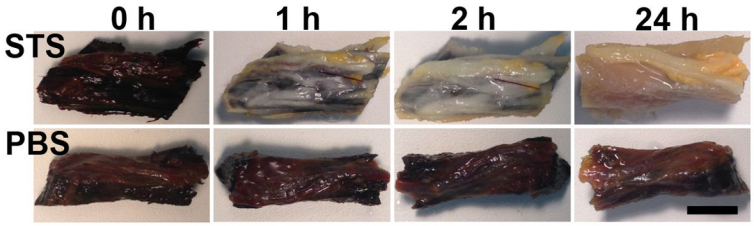

Figure 2.

Removal of Lugol's iodine with STS. Pieces of one adult rat sciatic nerve, including some surrounding muscle and connective tissue, were treated with Lugol's iodine solution (first column) and then rinsed in parallel with either sodium thiosulfate (STS) solution (top row) or PBS (bottom row) for the specified times. Bar = 3 mm.

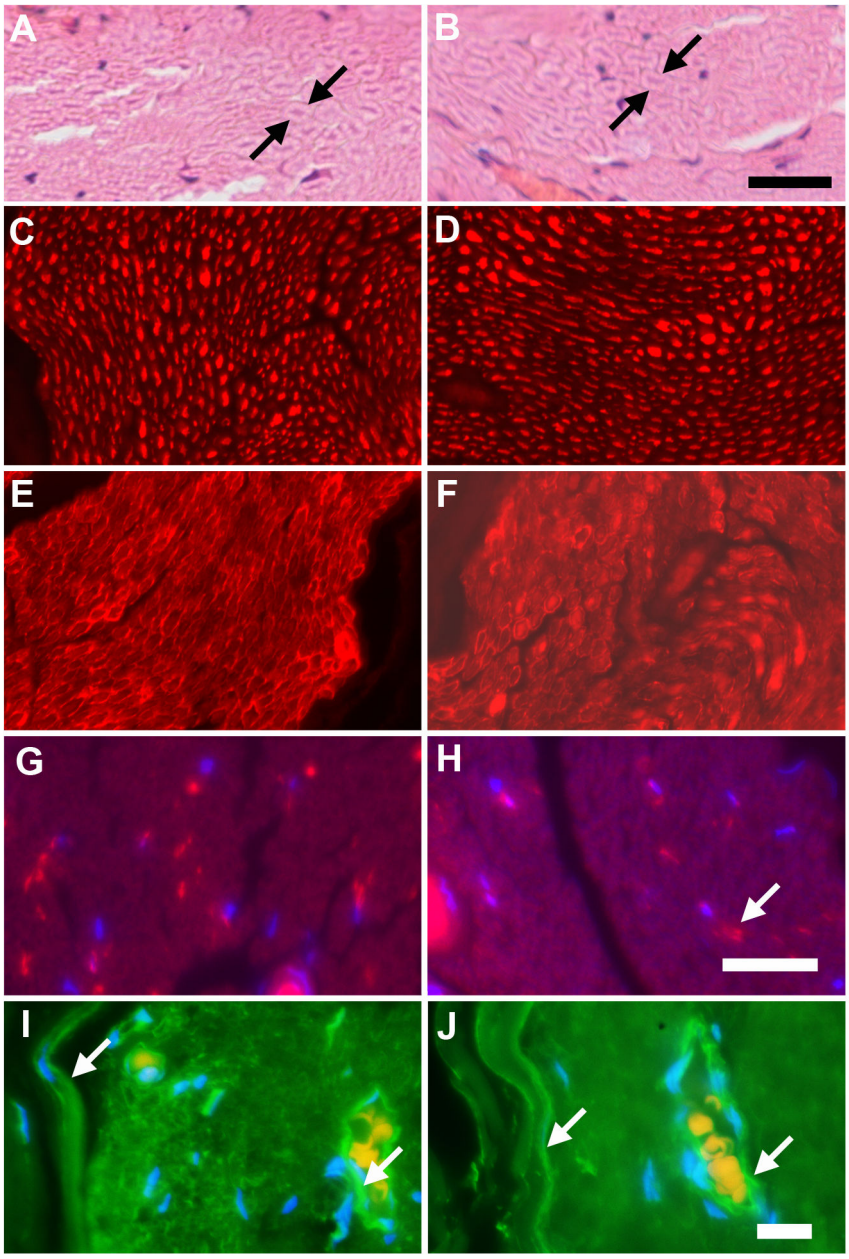

Figure 3.

Staining after iodine and STS. Fixed normal sciatic nerve pieces were treated in parallel with either PBS (A,C,E,G,I) or Lugol's solution and STS (B,D,F,H,J), embedded in paraffin, sectioned and stained with H&E (A, B, arrows point out single myelinated axons) or immunostained for axons (anti-NF, red staining, C, D), Schwann cells (anti-S100, red staining, E, F), blood vessels (fluorescent labeled lectin, red staining, G, H, arrow in H), nuclei (DAPI, blue staining in G, H, I, J) or cells expressing high levels of GLUT-1 (anti-GLUT-1, green, I, J, arrows point to the perineurium (left) and a blood vessel (right) in each). No differences were observed due to treatment. The bar in B = 25 μm and applies to A. The bar in H = 25 μm and applies to C–H. The bar in J = 25 μm and applies to I.

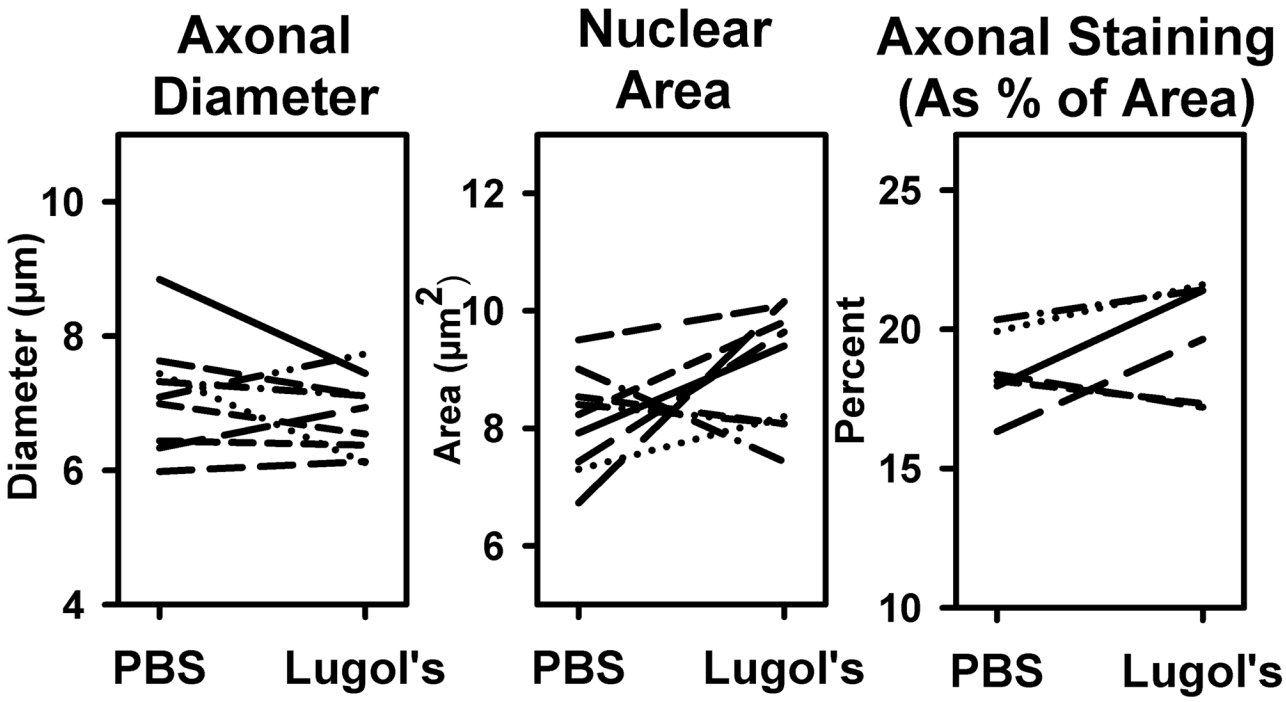

Figure 4.

Quantification of effects of Lugol's and STS on tissue morphology. A paired analysis on stained tissues from the same animal, treated with PBS or Lugol's/STS showed no significant differences using a repeated measures ANOVA ($p > 0.05$). The corresponding plots are shown for the effects of treatment on axonal diameter (from H&E stained sections, left), nuclear area (from DAPI stained sections, middle) and the percent of image area covered by NF immunostaining (from anti-NF labeled sections, right).

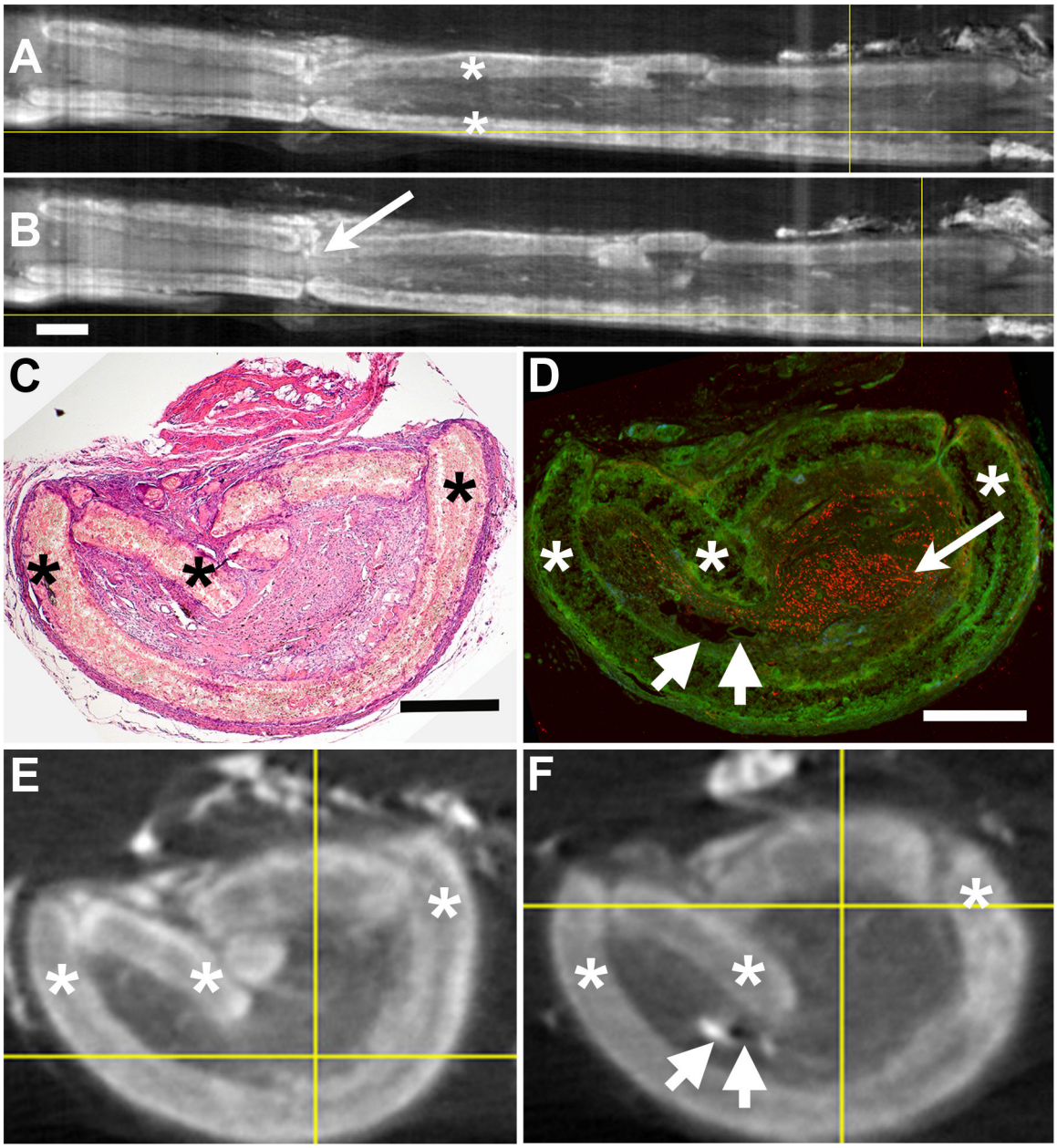

Figure 5.

Regenerated tissues growing through a PCL nerve conduit. (A) and (B) are longitudinal reconstructions of a nerve conduit containing regenerating sciatic nerve tissues after Lugol's iodine infiltration. The conduit material (asterisks) can be clearly differentiated from the proximal (left) and distal (right) nerve stumps and the internal regenerating nerve tissues (bar = 1 mm, applies to A and B). The arrow in B points to regenerated tissues. After iodine removal with STS, an H&E stained section (C) was matched to the corresponding axial micro-CT image (E) and a section stained with anti-NF (D, red staining was matched to the axial micro-CT image (F). Asterisks label conduit. The long arrow in D points to a group of

stained axons and short arrows in D and F point to a small pocket of fat (left) and a large blood vessel (right). Bars = 0.5 mm and apply to matching sections (C to E, D to F).

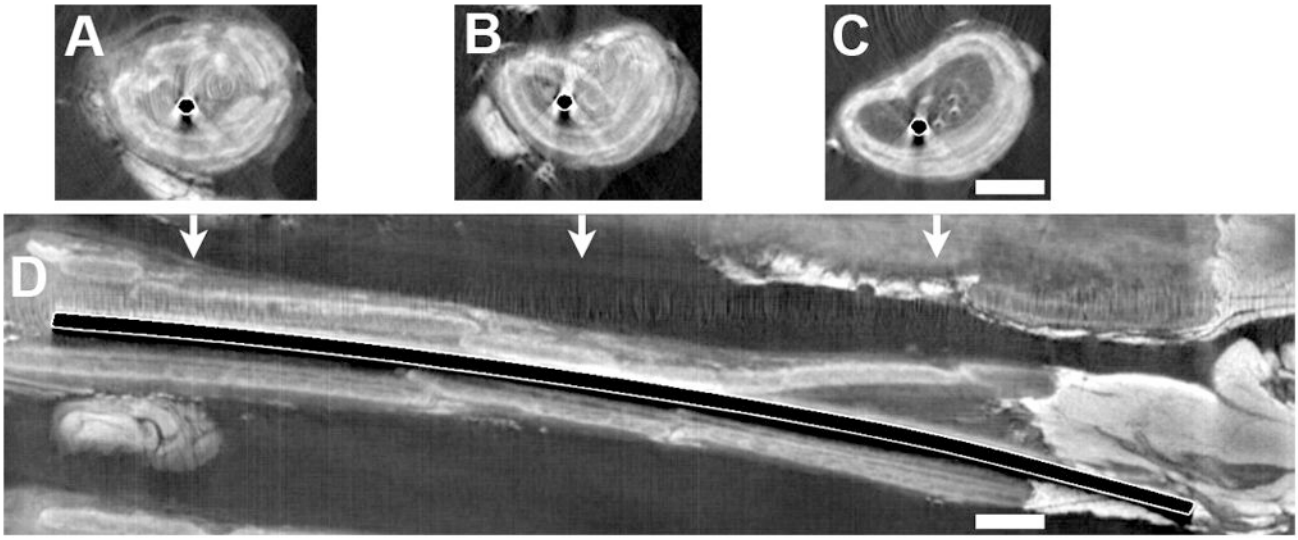

Figure 6.

Visualization of dense and iodine-enhanced soft tissues. After replacing a nerve gap with a conduit containing a Ti wire, the tissues were treated with iodine and micro-CT. Images are shown of selected axial slices (A–C) and the reconstructed longitudinal view (D). The axial images are placed above their approximate positions along the conduit from proximal (left) to distal (right). The conduit can be identified and differentiated from the internal and external tissues and the metal. Bars = 1 mm and apply to all images.